

# Design and Development of Advanced Cavity-Based Dual-Mode Filters Using Low-Temperature Co-Fired Ceramic Technology for V-band Gigabit Wireless Systems

Jong-Hoon Lee, *Student Member, IEEE*, Stephane Pinel, *Member, IEEE*, Joy Laskar, *Fellow, IEEE*, Manos M. Tentzeris, *Senior Member, IEEE*

**Abstract**— In this paper, a novel concept of three dimensional integrated V-band dual-mode cavity filters, which permit the realization of a variety of quasi-elliptic responses by creating transmission zeros, has been demonstrated using multilayer low-temperature co-fired ceramic technology. A single cavity resonator is designed to generate a degenerate resonance of two orthogonal modes ( $TE_{102}$  and  $TE_{201}$ ), enabling dual-mode operation. The appearance and elimination of transmission zeros have been analyzed through the multi-path coupling diagrams and lumped elements models. Then, the quasi-elliptic, dual-mode filters with the appropriate locations of the transmission zeros are developed for receiver and transmitter channels of a V-band transceiver module. Two pre-synthesized, dual-mode cavity filters are vertically stacked with two types of inter-coupling slots (1. rectangular 2. cross) to realize the multi-pole filters for 60 GHz wireless local area network narrowband applications. These proposed filters are the first to be reported and have great potential to be integrated into miniaturized V-band low-temperature co-fired ceramic transceiver modules.

**Index Terms**—Dual-mode, cavity filter, bandpass filter (BPF), system-on-package, millimeter wave, three-dimensional integration, even-mode, odd-mode, V-band, transceiver, low-temperature co-fired ceramic (LTCC), front-end module.

## I. INTRODUCTION

THE substantial advances in system-level packaging technology [1]-[2] and the immense research effort in 60GHz circuits design technology [3]-[9], [30]-[31] have stimulated the development of 60 GHz transceiver modules for wireless personal area network (WPAN) applications over past years. As the demand for compact and low-loss bandpass filters (BPFs) increases in 60 GHz multi-gigabit-per-second wireless transceiver systems, integrating on-package cavity

filters using multi-layer low-temperature co-fired ceramic (LTCC) technology has emerged as an attractive solution, due to their relatively high quality factor  $Q$  and power handling capability compared to planar filter structures, and less interference from other circuits integrated in the package [5]-[6], [31]. To achieve optimum frequency selectivity with a compact size and reduced weight, dual-mode dielectric rectangular [10]-[17] and circular waveguide filters [18]-[21] have been proposed, and their basic features are well understood. However, the proposed dual-mode techniques not only impose a very heavy numerical burden to the modal characterization of waveguides because of the large number of evanescent modes, but also are not applicable to LTCC multilayer processes because of the fabrication limitations against a solid metal wall. In the 60GHz band, the authors previously developed the single-mode cavity resonators [31] and three-pole BPFs [6], [31] by adopting the vertically deployment of three single-mode cavity resonators. However, these single-mode devices could not satisfy optimum frequency selectivity with a compact size and reduced weight. A dual-mode, stripline bandpass filter (BPF), which is integrated into LTCC system-in-packaging system, has been presented [22] at 60 GHz, but it requires complicated transitions using air cavities and staggered via structures, resulting in a relatively high insertion loss.

In this paper, the authors expand previous work to a new class of three-dimensional V-band dual-mode cavity filters and vertically stacked multi-pole filters using LTCC technologies, which enable a variety of quasi-elliptic responses by controlling the locations of transmission zeros. In Section II, a dual-mode single cavity filter is developed for receiver (Rx) and transmitter (Tx) channels through the offset of feeding structures and a cross coupling by source-to-load distance. In order to provide the additional design guideline for the multi-pole cavity filters, the vertically stacked arrangement of two dual-mode cavities is reported for the first time ever in Section III. The pre-synthesized dual-mode single cavity filters are stacked with two different coupling slots (rectangular and cross) between the two cavities. The feasibility of realizing a multi-pole filter has been validated with the experimental data.

Manuscript received Sept. 30, 2006. This work was supported by the Asahi Glass Company, by the Georgia Electronic Design Center, by the National Science Foundation (NSF) under NSF CAREER Award ECS-9984761, and by the NSF under Grant ECS-0313951.

J. -H. Lee, S. Pinel, J. Laskar, M. M. Tentzeris are with Georgia Electronic Design Center, School of Electrical and Computer Engineering, Georgia Institute of Technology, Atlanta, GA 30332 (e-mail: [jonglee@ece.gatech.edu](mailto:jonglee@ece.gatech.edu); [pinel@ece.gatech.edu](mailto:pinel@ece.gatech.edu); [joy.laskar@ece.gatech.edu](mailto:joy.laskar@ece.gatech.edu); [etentzeris@ece.gatech.edu](mailto:etentzeris@ece.gatech.edu)).

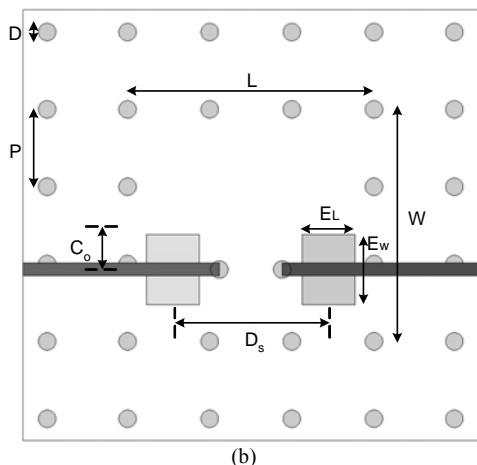
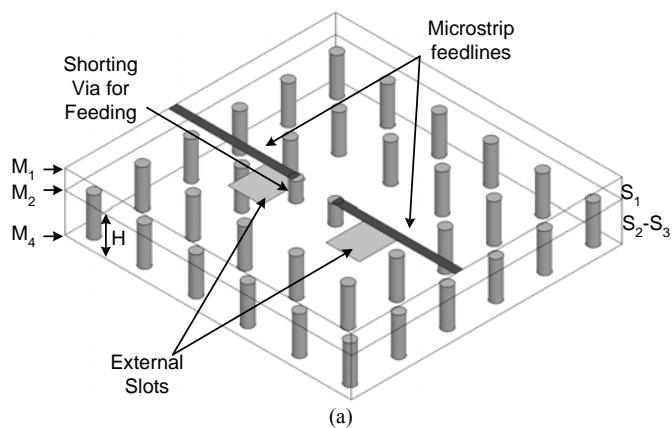


Figure 1. (a) The three dimensional overview (b) The top view of a quasi-elliptic dual-mode single cavity filter from [30].

## II. DUAL-MODE CAVITY FILTERS

### A. Single Dual-Mode Cavity Resonator

The square-shaped cavity resonator is first designed at a center frequency of 63 GHz to exhibit a degenerated resonance of two orthogonal modes ( $TE_{102}$  and  $TE_{201}$ ) characteristic of the dual-mode operation. LTCC multilayer substrates have been used for the fabrication, and its properties are as follows: The relative permittivity  $\epsilon_r$  is 7.1, loss tangent  $\tan\delta$  is 0.0017, the dielectric layer thickness is 53  $\mu\text{m}$  per layer for a total of 5 layers, the metal thickness is 9  $\mu\text{m}$ , and the resistivity of the metal (silver trace) is  $2.7 \times 10^{-8} \Omega \cdot \text{m}$ . Fig. 1 shows (a) the three dimensional overview and (b) the top view of the proposed structure. The dual-mode cavity resonator consists of one cavity occupying two substrate layers  $S_2$ - $S_3$ , the input/output (I/O) microstrip feedlines on  $M_1$  and the two coupling slots etched on the top ground plane,  $M_2$  of the cavity. The microstrip lines are terminated with a physical short circuit realized by a metallic via (throughout  $S_1$ ) to maximize the magnetic coupling through the slots. In order to determine the effective length,  $L$ , and width,  $W$ , in Fig. 1 (b) of the cavity resonator providing two orthogonal modes of  $TE_{102}$  and  $TE_{201}$ , both modes are constrained to resonate at the same frequency using the conventional resonant frequency equation of the rectangular waveguide cavity [15], [23]. The final dimensions

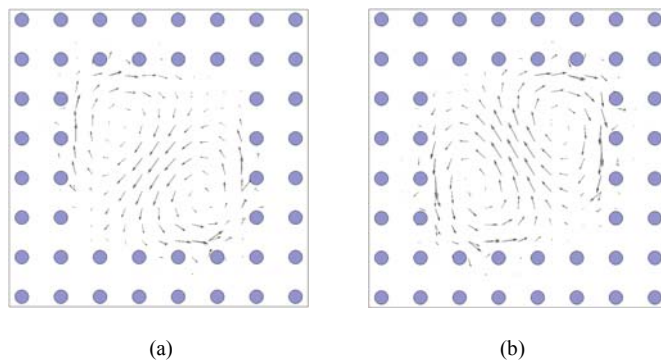


Figure 2. (a) Magnetic vector of the odd mode (b) Magnetic vector of the even mode

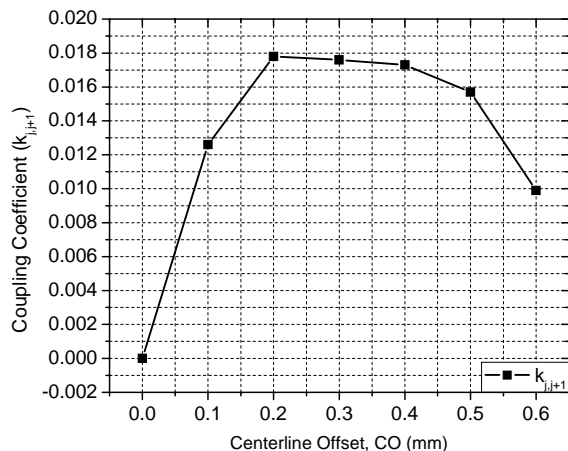


Figure 3. Internal coupling coefficient  $k_{j,j+1}$  as a function of the centerline offset  $C_o$  of the feeding structures.

of the cavity resonator using via fences as vertical walls are determined to be  $2.06 \times 2.06 \times 0.106 \text{ mm}^3$  in HFSS full-wave simulator first to resonate at 63 GHz. The size and spacing of the via posts are properly chosen according to the LTCC design rules, such as a minimum value of center-to-center vias spacing  $p$  in Fig. 1 (b) of 390  $\mu\text{m}$  and a minimum value of via diameter  $d$  in Fig. 1 (b) of 145  $\mu\text{m}$ .

### B. Internal Coupling

The centerline offset,  $C_o$ , in Fig. 1 (b) between the feeding structure and cavity position is one of major factors in realization of the dual-mode operation and controlling the mutual internal coupling of the modes, hence providing transmission zeros at the desired positions for a high selectivity. When the I/O slots are centered at the cavity interface ( $C_o=0$  mm), only the  $TE_{102}$  mode is excited so that the transmission zeros do not exist. However, when a transverse offset,  $C_o$ , is applied to the position of the I/O feeding structure, the additional mode,  $TE_{201}$ , is excited. This mode degeneration can be used to realize dual-mode filters. The basis modes are defined as even and odd mode, respectively [24], (by vectorial addition and subtraction of  $TE_{102}$  and  $TE_{201}$  modes) and the magnetic vectors of these modes calculated using HFSS simulation software are displayed in Fig. 2. These resonant

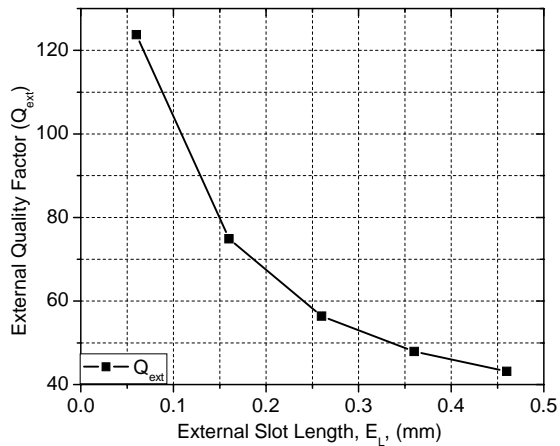


Figure 4. External quality factor  $Q_{ext}$  evaluated as a function of external slot length  $E_L$ .

frequencies ( $f_e$ : even mode,  $f_o$ : odd mode) are associated to the inter-coupling coefficient according to the definition of the ratio of the coupled energy to the stored energy of an uncoupled single resonator [25]. The value of  $f_e$  ( $f_o$ ) can be derived from a symmetric structure by placing a perfect electric conductor (a perfect magnetic conductor) on the plane of the symmetry. Fig. 3 displays the internal coupling coefficient as a function of the variation of the centerline offset  $C_o$ .

### C. External Coupling

The I/O external slots on the top ground plane of the cavity are designed for the magnetic excitation of the cavity from the 50  $\Omega$  microstrip lines. The accurate design of the external coupling slots that is directly related to the external quality factor,  $Q_{ext}$ , is a key issue to achieve a high- $Q$  cavity resonator. The  $Q_{ext}$  corresponds to the resistance and the reactance and can be controlled by the position and size of the coupling slots. In order to investigate how the slot size affects the  $Q_{ext}$ , the external slots are initially placed at a quarter of the cavity length from the (front and back) edge of the cavity, and the slot length is varied with the fixed slot width ( $\sim \lambda_g/4$ ). The issues related to the distance between external slots ( $D_s$  in Fig. 1) will be discussed in detail in section D. Both single-mode case ( $C_o=0mm$ ) and dual-mode case ( $C_o = 0.6mm$ ) were tested. In the single mode case, the  $Q_{ext}$  can be determined by the relation [25] between the resonant frequency and the frequencies where a  $\pm 90^\circ$  phase response in  $S_{11}$  parameter is exhibited. However, in the dual-mode case, the external coupling factor is directly related to the internal coupling coefficient according to the analytical equation [26]

$$Q_{ext} = \frac{1}{\sqrt{k_{1,2}^2 - k_{(1,2)wo}^2}} \quad (1)$$

where  $k_{1,2}$  is the coupling coefficient of the dual-mode resonator with an external circuit and  $k_{(1,2)wo}$  is the coupling

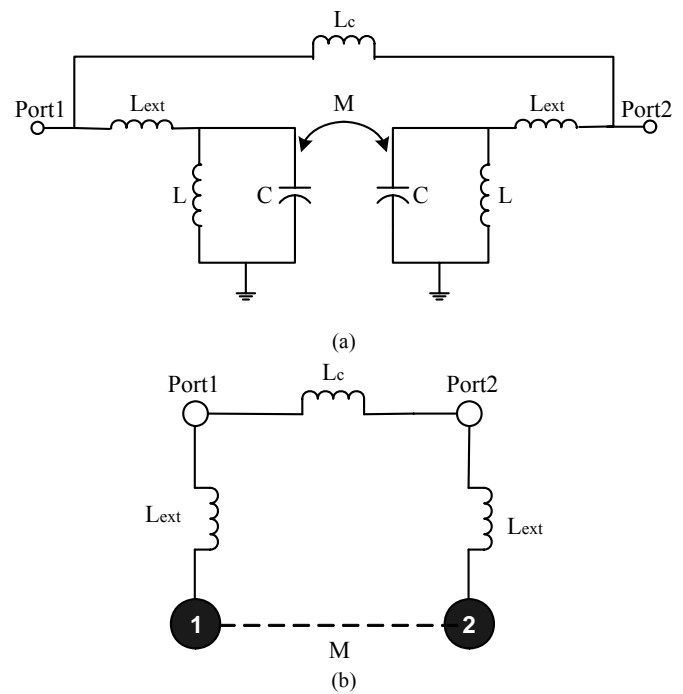


Figure 5. (a) Equivalent circuit model of the quasi-elliptic dual-mode cavity filter (b) Multi-coupling diagram for the quasi-elliptic dual-mode cavity filter

TABLE I  
TOTAL PHASE SHIFTS FOR TWO DIFFERENT PATHS IN THE DUAL-MODE CAVITY FILTER

Paths	Below Resonance	Above Resonance
Port1-1-2-Port2	$-90^\circ + 90^\circ + 90^\circ + 90^\circ - 90^\circ = +90^\circ$	$-90^\circ - 90^\circ + 90^\circ - 90^\circ - 90^\circ = -270^\circ$
Port1-Port2	$-90^\circ$	$-90^\circ$
Result	Out of Phase	Out of Phase

coefficient of the dual-mode resonator without an external circuit.

Fig. 4 shows the relationship between the length variation of the external slots  $E_L$  and the  $Q_{ext}$  from the simulation when the feeding structure is placed at 0.6mm away from the center of the cavity ( $C_o = 0.6mm$ ). A larger  $E_L$  results in smaller  $Q_{ext}$  that is interpreted as a stronger external coupling.

### D. Transmission Zeros

In this section, the dual-mode filter realization with transmission zeros for high selectivity will be discussed. The equivalent circuit model of the proposed dual-mode cavity filter is shown in Fig. 5 (a). The filter consists of major four sections: (1) a pair of LC resonators that represent each of the degenerate dual modes in the cavity resonator, (2) mutual internal electric coupling,  $M$ , between a pair of parallel LC resonators, (3) external magnetic coupling,  $L_{ext}$  from each of the I/O external slots, and (4) magnetic cross coupling,  $L_c$ , representing the parasitic source to load coupling associated with the perturbed electric fields in the cavity [32]. A pair of transmission zeros at the upper and lower sides of the passband can be created when  $L_c$  has a  $180^\circ$  phase difference with respect

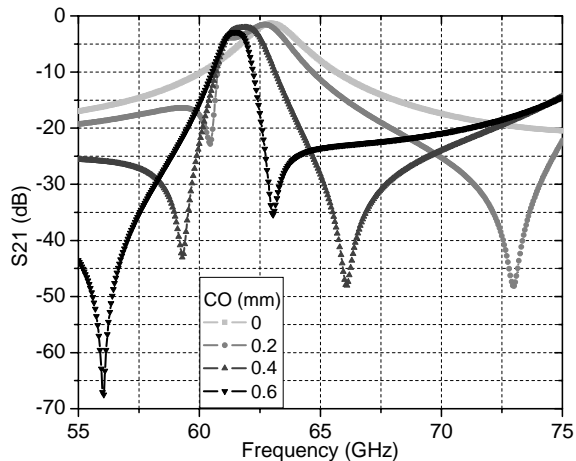


Figure 6. The simulated  $S_{21}$  parameter response of a dual mode filter as a function of the centerline offset  $C_o$  of the feeding structures.

to  $M$  with similar magnitudes. This sign reversal is attributed to a destructive interference between two modes, therefore, resulting in the construction of transmission zeros at two frequencies. The fundamental cross coupling technique is well explained in [27] by using multipath coupling diagrams to illustrate the relative phase shifts of multiple single paths. In [27], Brian adopted the  $S_{21}$  phase shift,  $\Phi_{21}$ , of each lumped element in the equivalent circuits of a resonator and calculated the total phase shift at the input (or output) of the resonator to predict the behavior of transmission zeros. Since transmission zeros appear away from the passband, the off-resonance behavior of each lumped component is of concern. Based on Brian's theory, the equivalent circuit for a dual-mode cavity filter can be represented by a multi-path diagram as described in Fig. 5 (b). The shunt capacitor/inductor pairs of the equivalent circuit have been replaced by the black circles, and  $M$  represents the mutual electric coupling between two modes. The phase shift of each lumped element is used to calculate the total phase shift at the input or output of the filter for the different signal paths. In the case of the dual-mode single cavity filter, there are two possible signal paths (1) *path1: Port1-1-2-Port2* and (2) *path2: Port1-Port2*. Both paths share the common input (*Port1*) and output (*Port2*). The total phase shifts for two signal paths in the dual-mode cavity are summarized in Table I. The total phase shift for path 1 is  $-90^\circ$  both below and above resonance. The total phase shift for *path 2* only accounts for the cross magnetic coupling  $L_c$  between *port1* and *port2*, hence being  $+90^\circ$ . Therefore, two paths are out of phase both below and above resonance, meaning that destructive interferences creating transmission zeros occur both below and above the passband.

The locations of the upper and lower stopband transmission zeros for the filter can be controlled by adjusting the values of  $M$  and  $L_c$  through varying the centerline offset,  $C_o$ , and distance,  $D_s$ , between the *I/O* external slots, respectively.

Shown in Fig. 6 are the simulated responses of a dual mode filter as a function of the parameter,  $C_o$ . When the feeding

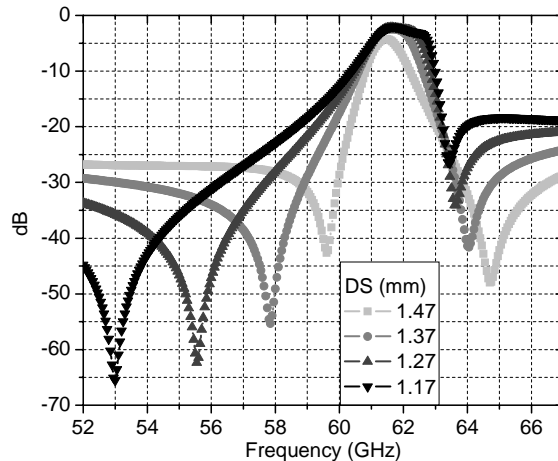


Figure 7. The simulated  $S_{21}$  parameter response of a dual mode filter as a function of the source-to-load distance  $D_s$ .

structure is placed at the center of the cavity ( $C_o=0$  mm), only the  $TE_{102}$  mode is excited, producing no transmission zeros. As  $C_o$  increases, the level of internal electric coupling,  $M$ , influences the upper transmission zeros more than the lower transmission zeros because of the asymmetrical effect of  $M$  upon the upper and lower poles [28]. The centerline offset,  $C_o$ , affects the performance of the 3-dB bandwidth and center frequency as well. It is observed that the maximum 3-dB bandwidth is obtained at the offset of 0.2 mm with the maximum coupling between dual modes. Further increase of the offset results in a narrower bandwidth because the level of coupling for  $TE_{102}$  and  $TE_{201}$  changes. The downward shifting of the center frequency could be caused by the difference between the mean frequency ( $(f_o + f_e)/2$ ) and the original resonant frequency of the cavity resonator. Also, external coupling can be attributed to the center frequency shift because of its additional reactance effect from the feeding structures.

The transmission characteristic of the filter is investigated with respect to the values of  $L_c$  by varying the distance  $D_s$  with a fixed centerline offset,  $C_o=0.5$  as shown in Fig. 7. As  $L_c$  decreases by increasing  $D_s$ , the lower transmission zero shifts away from the center frequency while the higher transmission zero moves toward to the center frequency. The cross coupling,  $L_c$ , causes the asymmetrical shift of both transmission zeros due to the same reason mentioned in the case of  $M$ , influencing the lower transmission zero more than the higher one. Our equivalent-circuit models are justified to validate the coupling mechanisms through the design of a transmitter filter in the next sub-section.

#### E. Quasi-Elliptic Dual-Mode Cavity Filter

Two dual-mode cavity filters exhibiting a quasi-elliptical response are developed as the next step for a three dimensional integrated V-band transceiver front-end module. The frequency range of interest is divided into two channels where the lower channel is allocated for a receiver (Rx), and the higher channel allocated for a transmitter (Tx). To suppress the

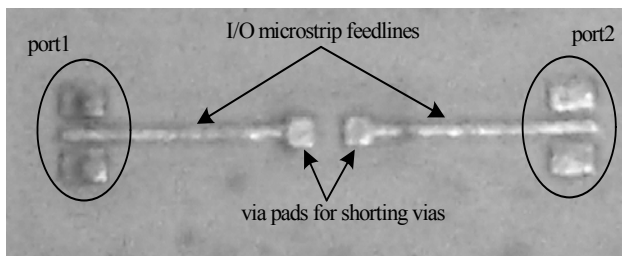


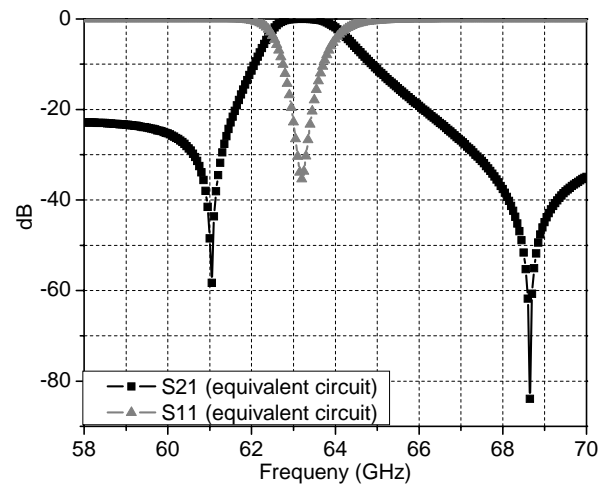
Figure 8. The photograph of the fabricated input/output microstrip feedlines with an open stub and CPW probe pads utilized to excite the embedded the cavity resonator

interference between the two channels as much as possible, the upper stop-band transmission zero of the Rx channel is placed closer to the center frequency of the passband than the lower stop-band zero. In the case of a Tx filter, the lower zero is located closer to the center frequency of the passband than the upper zero.

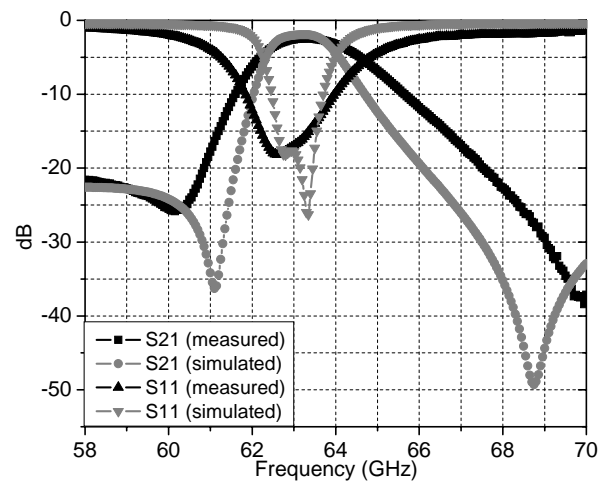
First, a Rx filter was designed and validated with experimental data in our previous work [31]. All of the fabricated resonators were measured using the Agilent 8510C Network Analyzer and Cascade Microtech probe station with 250 μm pitch air coplanar probes, and the photograph of a device is shown in Fig. 8. A line-reflect-reflect-match (LRRM) method [29] was employed for calibration. In the measurement, the reference planes are decided to be at the end of the probing pads, and the capacitance and inductance effects of the probing pads are de-embedded by use of “Wincal” software so that effects, such as those due to the CPW loading, become negligible. The filter exhibits an insertion loss of <2.76 dB, center frequency of 61.6 GHz, and 3-dB bandwidth of about 4.13 % (≈ 2.5 GHz). The upper and lower transmission zeros are observed to be within 3.4 GHz and 6.4 GHz away from the center frequency, respectively.

Then, a Tx filter using a dual-mode cavity resonator is designed for a center frequency of 63.4 GHz, fractional 3-dB bandwidth of 2%, insertion loss of <3dB, and 25dB rejection BW on the lower side of the passband of <2GHz. To obtain a center frequency of 63.4 GHz, the size of the via-based cavity is adjusted and determined to be 2.04×2.06×0.106 (L×W×H in Fig.1) mm<sup>3</sup>. The corresponding lumped-element values in the equivalent-circuit model (Fig. 5 (a)) of a Tx filter are evaluated, and their values are L<sub>ext</sub> = 0.074 nH, L = 0.0046 nH, C = 1.36 pF, M = 0.032 pF and L<sub>c</sub> = 0.73 nH. Fig. 9 (a) shows the ideal response from the circuit model, exhibiting two transmission zeros at 61.6 and 68.7 GHz.

The measured insertion loss and reflection losses of the fabricated filter are compared to the full-wave simulation results in Fig. 9 (b). The fabricated Tx filter exhibits an insertion loss of 2.43 dB, which is slightly higher than the simulated (2.0 dB). The main source of this discrepancy might be caused by the skin and edge effects of the metal traces since the simulations assume a perfect definition of metal strips with finite thickness. The center frequency is measured to be 63.4 GHz. The upper and lower transmission zeros are observed to be within 6.5 GHz and 3.2 GHz away from the center frequency, respectively. Those can be compared to the simulated values that exhibit the upper and lower transmission zeros within less



(a)



(b)

Figure 9. (a) Simulated S-parameters of the dual-mode cavity filter using equivalent-circuit model in Fig. 6 (a). (b) Measured and simulated S-parameters of the dual-mode cavity filter for a Tx channel.

TABLE II  
DESIGN PARAMETERS OF QUASI-ELLIPTIC DUAL-MODE CAVITY FILTERS

Design Parameters	Rx Filter(mm)	Tx Filter(mm)
cavity length ( <i>L</i> )	2.075	2.04
cavity width ( <i>W</i> )	2.105	2.06
cavity height ( <i>H</i> )	0.106	0.106
external slot length ( <i>E<sub>l</sub></i> )	0.360	0.360
external slot width ( <i>E<sub>w</sub></i> )	0.572	0.572
centerline offset ( <i>Co</i> )	0.5675	0.35
distance bet. external slots ( <i>D<sub>s</sub></i> )	1.37	1.355

than 5.3 GHz and 2.3 GHz away from the center frequency. The discrepancy of the zero positions between the measurement and the simulation can be attributed to the fabrication tolerance. Also, the misalignment between the substrate layers in the LTCC process might cause an undesired offset of the feeding structure position. This could be another major contribution to a transmission zero shift. These

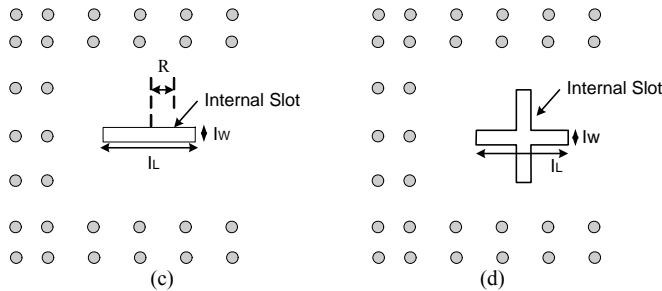
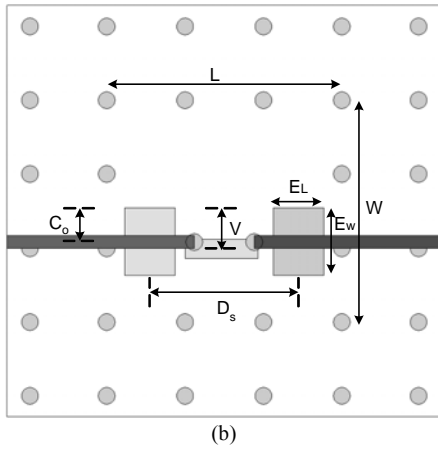
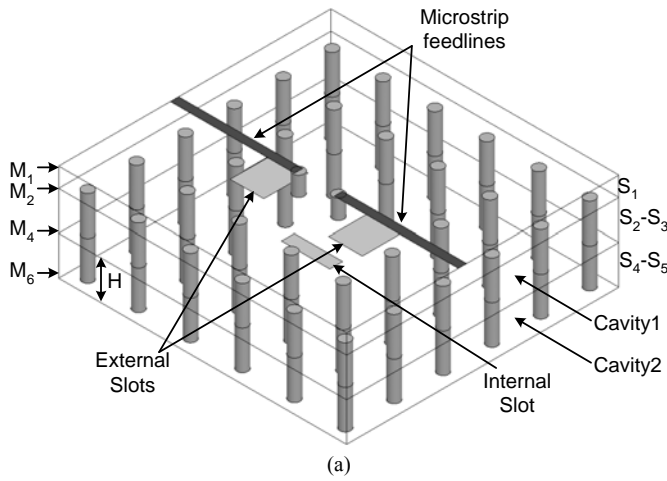


Figure 10. (a) The three-dimensional overview (b) The top view of a vertically stacked multi-pole dual-mode cavity filter (c) Inter-coupling rectangular slot (d) Inter-coupling cross slot.

fabrication tolerances also result in the bandwidth differences. The filter exhibits a 3-dB measured bandwidth of 4.02 % (~2.5 GHz) compared to the simulated one of 2 % (~1.3 GHz). All of the final layout dimensions optimized using HFSS are summarized in Table II.

### III. MULTI-POLE DUAL-MODE CAVITY FILTERS

In order to provide the additional design guidelines for generic multi-pole cavity filters, the authors proceed with a vertically stacked arrangement of two dual-mode cavities. The pre-synthesized dual-mode cavities are stacked with a coupling slot in order to demonstrate the feasibility of realizing a multi-pole filter by using the dual-mode cavity filters investigated in Section II. Two well-known types of slots

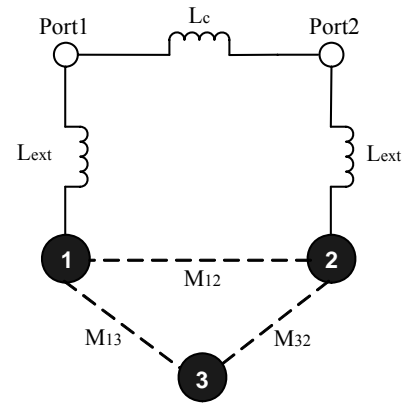


Figure 11. Multi-coupling diagram for the vertically stacked multi-pole dual-mode cavity filter with rectangular slot for inter-coupling between two cavities.

TABLE III  
TOTAL PHASE SHIFTS FOR THREE DIFFERENT SIGNAL PATHS IN THE VERTICALLY STACKED DUAL-MODE CAVITY FILTER WITH A RECTANGULAR SLOT

Paths	Below Resonance	Above Resonance
Port1-1-2-Port2	$-90^\circ+90^\circ+90^\circ+90^\circ-90^\circ=+90^\circ$	$-90^\circ-90^\circ+90^\circ-90^\circ-90^\circ=-270^\circ$
Port1-Port2	$-90^\circ$	$-90^\circ$
Result	Out of Phase	Out of Phase
1-3-2	$-90^\circ+90^\circ-90^\circ=-90^\circ$	$-90^\circ-90^\circ-90^\circ=-270^\circ$
1-2	$+90^\circ$	$+90^\circ$
Result	Out of Phase	In Phase

(rectangular and cross-shaped) are considered as the inter-coupling structure in this study. HFSS was employed to optimize the size and the position of the inter-coupling slots for the desired frequency response. The three-dimensional overview (a), top view (b), inter-coupling rectangular slot (c) and inter-coupling cross slot (d) of the proposed cavity filter are illustrated in Fig. 10. The top five substrate layers (Microstrip line:  $S_1$ , Cavity1:  $S_2-S_3$ , Cavity2:  $S_4-S_5$ ) are occupied by the filter. Two identical dual-mode cavity resonators (Cavity1 and Cavity2) are vertically stacked and coupled through an inter-coupling slot to achieve the desired frequency response with high selectivity as well as a high-level of compactness.

#### A. Quasi-Elliptic Filter with a Rectangular Slot

The multi-path diagram of a vertically stacked dual-mode filter with a rectangular slot is illustrated in Fig. 11. The black circles denoted by 1 and 2 are the degenerate resonant modes in the top dual-mode cavity while the one denoted by 3 represents the excited resonant mode in the bottom cavity. The coupling  $M_{12}$  is realized through the electrical coupling and controlled by the offsets of the I/O feeding structures. Also, the inter-couplings,  $M_{13}$  and  $M_{32}$ , are determined by the sizes and positions of the inter-coupling slots and dominated by the magnetic coupling. It is worth noting that  $M_{13}$  is different from  $M_{32}$  since the magnitude of the magnetic dipole moment of each mode in a coupling slot is different to each other due to the

TABLE IV  
DESIGN PARAMETERS OF MULTI-POLE DUAL-MODE CAVITY FILTERS WITH TWO TYPES OF INTER-COUPLING SLOTS

Design Parameters	Rectangular(mm)	Cross (mm)
cavity length ( $L$ )	2.04	2.06
cavity width ( $W$ )	1.92	2.06
each cavity height ( $H$ )	0.106	0.106
external slot length ( $E_L$ )	0.440	0.470
external slot width ( $E_W$ )	0.582	0.472
centerline offset ( $Co$ )	0.245	0.356
internal slot length ( $I_L$ )	0.642	0.412
internal slot width ( $I_W$ )	0.168	0.145
vertical slot offset ( $V$ )	0.325	0.6075
horizontal slot offset ( $R$ )	0.065	0
distance between external slots ( $D_s$ )	1.29	1.26

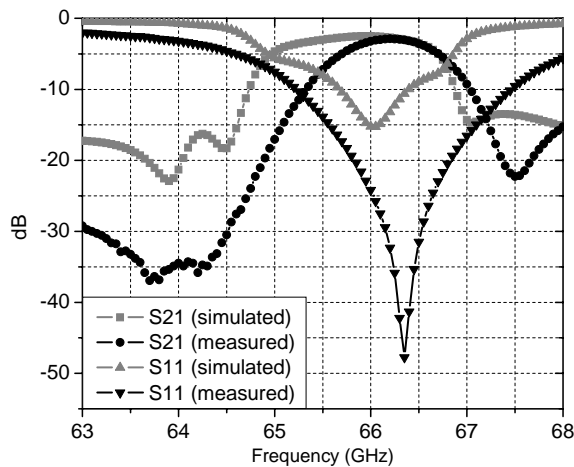


Figure 12. Measured and simulated  $S$ -parameters of the quasi-elliptic dual-mode cavity filter with a rectangular slot for inter coupling between cavities.

nature of a rectangular slot. Since the rectangular slot is parallel to the horizontal direction, the modes polarized to the horizontal direction are more strongly coupled through the slot than the other modes that are polarized in the vertical direction. However, by adjusting the offset, the authors attempted to obtain the appropriate coupling level of  $M_{13}$  and  $M_{32}$  to realize the desired filter response.  $L_c$  (the magnetic coupling parameter) is used to implement the cross coupling between  $Port1$  and  $Port2$ . The phase shifts for three possible signal paths are summarized in Table III. The filter with three modes can generate two transmission zeros below resonance and an additional zero above resonance.

The three-pole quasi-elliptic filters were designed to meet the following specifications: (1) center frequency: 66 GHz, (2) 3-dB fractional bandwidth:  $\sim 2.6\%$ , (3) insertion loss:  $< 3$  dB, and (4) 15 dB rejection bandwidth using triple transmission zeros (two on the lower side and one on the upper side):  $< 3$  GHz. A study of the dual-mode coupling in each cavity on the basis of the initial determination of the cavity size resonating at a

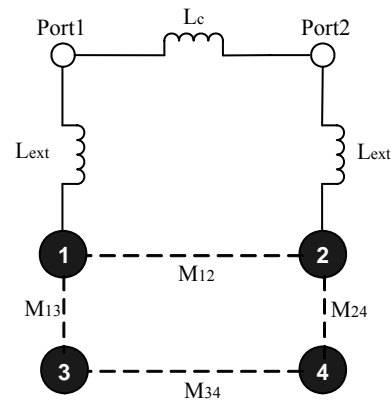


Figure 13. Multi-coupling diagram for the vertically stacked multi-pole dual-mode cavity filter with cross slot for inter-coupling between two cavities.

TABLE V  
TOTAL PHASE SHIFTS FOR THREE DIFFERENT SIGNAL PATHS IN THE VERTICALLY STACKED DUAL-MODE CAVITY FILTER WITH A CROSS SLOT

Paths	Below Resonance	Above Resonance
Port1-1-2-Port2	$-90^\circ + 90^\circ + 90^\circ + 90^\circ - 90^\circ = +90^\circ$	$-90^\circ - 90^\circ + 90^\circ - 90^\circ - 90^\circ = -270^\circ$
Port1-Port2	$-90^\circ$	$-90^\circ$
Result	Out of Phase	Out of Phase
1-3-4-2	$-90^\circ + 90^\circ + 90^\circ + 90^\circ - 90^\circ = +90^\circ$	$-90^\circ - 90^\circ + 90^\circ - 90^\circ - 90^\circ = -270^\circ$
1-2	$+90^\circ$	$+90^\circ$
Result	In Phase	In Phase

desired center frequency (66 GHz) is performed first. Then, the final configuration of the three-pole dual-band filter can be obtained through the optimization of the inter-coupling slot size and offsets via simulation. The determined design parameters were not sufficient to provide three notches on the simulated return loss because the relatively weak inter-couplings as shown in Fig. 12. All of the design parameters for the filters are summarized in Table IV.

Fig. 12 shows the measured performance of the designed filters with a rectangular slot along with a comparison to the simulated results. It can be observed that the measured results with a rectangular slot produce a center frequency of 66.2 GHz with the bandwidth of 1.2 GHz ( $\sim 1.81\%$ ), and the minimum insertion loss in the passband around 2.9 dB. The simulation showed a minimum insertion loss of 2.5 dB with a slightly wider 3-dB bandwidth of 1.7 GHz ( $\sim 2.58\%$ ) around the center frequency of 65.8 GHz. The center frequency shift is caused by an XY shrinkage of  $\pm 3\%$ . The two measured transmission zeros with a rejection better than 34 dB and 37 dB are observed within  $< 1.55$  GHz and  $< 2.1$  GHz, respectively, away from the center frequency at the lower band than the passband. One transmission zero is observed within  $< 1.7$  GHz at the higher band than the passband. This type of filter can be used to generate the sharp skirt at the low side to reject local oscillator and image signals, as well the extra transmission zero in the high skirt that can be utilized to suppress the harmonic

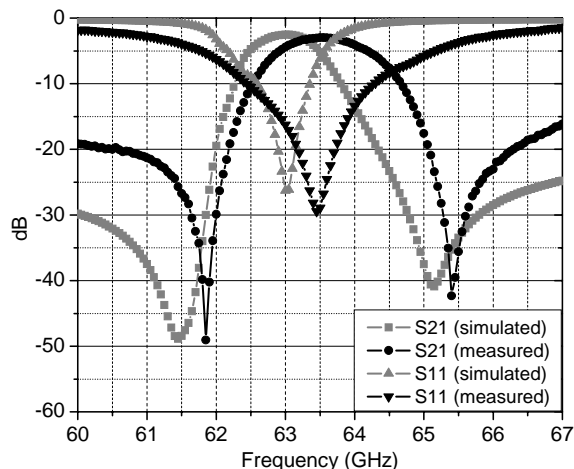


Figure 14. Measured and simulated S-parameters of the quasi-elliptic dual-mode cavity filter with a rectangular slot for inter coupling between cavities.

frequencies according to the desired design specification.

### B. Quasi-Elliptic Filter with a Cross Slot

The cross slot is applied as an alternative inter-coupling slot between the two vertically stacked cavities. The multi-paths diagram for the filter and the phase shifts for the possible signal paths are described in Fig. 13 and Table V, accordingly. Each cavity supports two orthogonal dual modes (1 and 2 in the top cavity, 3 and 4 in the bottom cavity) since the cross slot structure excites both degenerate modes in the bottom cavity by allowing the coupling between the modes that have the same polarizations. The coupling level can be adjusted by varying the size and position of the cross slots. The couplings of  $M_{12}$  and  $M_{34}$  are realized by electrical coupling while the inter couplings of  $M_{13}$  and  $M_{24}$  are realized by magnetic coupling. The total phase shifts of the four signal paths of the proposed structure prove that they generate one zero above resonance and one below resonance.

The quasi-elliptic filters were designed for a sharp selectivity, and the simulation achieved the following specifications: (1) center frequency: 63 GHz, (2) 3-dB fractional bandwidth:  $\sim 2\%$ , (3) insertion loss:  $< 3$  dB, and (4) 40 dB rejection bandwidth using two transmission zeros (one on the lower side and one on the upper side) :  $< 4$  GHz. The filter was fabricated using LTCC substrate layers, and Fig. 16 shows the measured results compared to those of the simulated design. The fabricated filter exhibits a center frequency of 63.5 GHz, an insertion loss of approximately 2.97 dB, a 3-dB bandwidth of approximately 1.55 GHz ( $\sim 2.4\%$ ), and  $> 40$  dB rejection bandwidth of 3.55 GHz.

## IV. CONCLUSION

In this work, three dimensional quasi-elliptic dual-mode single cavity filters and vertically stacked multi-pole cavity filters have been successfully developed using LTCC technology at 60 GHz. For the first time, the cavity-based

dual-mode filters were experimentally validated at V-band frequencies with excellent performance in terms of low insertion loss and high stop-band rejection. The quasi-elliptic dual mode filters are developed for Rx and Tx channels for a V-band transceiver module and exhibit very satisfactory characteristics with proper locations of transmission zeros. The pre-synthesized dual-mode cavities are stacked in order to demonstrate the feasibility of realizing multi-pole filters. The cross slot takes advantage of providing a high selectivity by exciting two degenerate modes in the bottom cavity but has some disadvantages of numerical and fabrication burden due to the design complexity compared to a rectangular slot. The proposed devices will be used as a complete passive front-end solution to be integrated into miniaturized V-band LTCC transceiver modules for V-band WPAN gigabit wireless communications.

## ACKNOWLEDGMENT

The authors wish to acknowledge the support of Asahi Glass Co., the Georgia Tech. Packaging Research Center, the Georgia Electronic Design Center, the NSF CAREER Award #ECS-9984761, and the NSF Grant #ECS-0313951.

## REFERENCES

- [1] M.M.Tentzeris, J.Laksar, J.Papapolymerou, S.Pinel, V.Palazzari, R.Li, G.DeJean, N.Papageorgiou, D.Thomson, R.Bairavasubramania, S.Sarkar and J.-H.Lee, "3D Integrated RF and millimeter-wave functions and modules using liquid crystal polymer (LCP) system-on-package technology," *IEEE Trans. on Advanced Packaging*, vol. 27, no. 2, pp. 332-340, May 2005.
- [2] R.R.Tummala, M.Swaminathan, M.M.Tentzeris, J.Laskar, G.-K.Chang, S.Sitaraman, D.Keezer, D.Guidotti, Z.Huang, K.Lim, L.Wan, S.K.Bhattacharya, V.Sundaram, F.Liu and P.M.Raj, "The SOP for miniaturized, mixed-signal computing, communication and consumer systems for the next decade," *IEEE Trans. on Advanced Packaging*, vol. 27, no.2, pp. 250-267, May 2004.
- [3] C.H.Doan, S.Emami, D.A.Sobel, A.M.Niknejad, and R.W.Brodersen, "Design Considerations for 60GHz CMOS Radios," *IEEE Communication Magazine*, vol. 42, no. 12, pp. 132-140, Dec 2004B. Smith, "An approach to graphs of linear forms (Unpublished work style)," unpublished.
- [4] K.Kornegay, "60GHz Radio Design Challenges," in *2003 GaAs IC Sym. Dig.*, San Diego, CA, Nov. 2003, pp. 89-92.
- [5] J.-H.Lee, G.DeJean, S.Sarkar, S.Pinel, K.Lim, J.Papapolymerou, J.Laskar, and M.M.Tentzeris, "Highly Integrated Millimeter-Wave Passive Components Using 3-D LTCC System-on-Package (SOP) Technology," *IEEE Transaction on Microwave Theory and Technique*, vol.53, no. 6, pp. 2220-2229, June 2005.
- [6] J.-H.Lee, N.Kidera, G.DeJean, S.Pinel, J.Laskar, and M.M.Tentzeris, "A V-band front-end with 3-D integrated cavity filters/duplexers and antenna in LTCC technologies," *IEEE Transaction on Microwave Theory and Technique*, vol.54, no. 7, pp. 2925-2236, July 2006.
- [7] Y.C.Lee, W.-I.Chang, Y.H.Cho, and C.S.Park, "A Very Compact 60GHz Transmitter Integrating GaAs MMICs on LTCC Passive Circuits for Wireless Terminals Applications," in *2004 IEEE MTT-S Int. Microwave Sym. Dig.*, Fort Worth, TX., Oct. 2004, pp. 313-316.
- [8] K.Ohata, K.Maruhashi, M.Ito, S.Kishimoto, K.Ikuina, T.Hashiguchi, K.Ikeda, and N.Takahashi, "1.25 Gbps Wireless Gigabit Ethernet Link at 60 GHz-Band," in *2003 IEEE MTT-S Int. Microwave Sym. Dig.*, Philadelphia, PA, June 2003, pp. 373-376.
- [9] J.Mizoe, S.Amano, T.Kuwabara, T.Kaneko, K.Wada, A.Kato, K.Sato, and M.Fujise, "Miniature 60 GHz Transmitter/Receiver Modules on AlN Multi-Layer High Temperature Co-Fired Ceramic," in *1999 IEEE MTT-S Int. Microwave Sym. Dig.*, Anaheim, CA, June 1999, pp. 475-478.

- [10] H.-C.Chang, K.A.Zaki, "Evanescent-mode coupling of dual-mode rectangular waveguide filters," *IEEE Transaction on Microwave Theory and Technique*, vol.39, no. 8, pp. 1307-1312, Aug. 1991.
- [11] K.Sano and M.Miyashita, "Application of the planar I/O terminal to dual-mode dielectric-waveguide filters," *IEEE Transaction on Microwave Theory and Technique*, vol.48, no. 12, pp. 2491-2495, Dec. 2000.
- [12] A.I.Atia and A.E.Williams, "Narrow-bandpass waveguide filters," *IEEE Transaction on Microwave Theory and Technique*, vol. MTT-20, no. 4, pp. 258-265, April 1972.
- [13] A.I.Atia and A.E.Williams, "Nonminimum-phase optimum-amplitude bandpass waveguide filters," *IEEE Transaction on Microwave Theory and Technique*, vol. MTT-22, no. 4, pp. 425-431, April 1974.
- [14] D.Deslandes and K.Wu, "Substrate Integrated Waveguide Dual-Mode Filters for Broadband Wireless Systems," in *2003 Radio and Wireless Conf.*, Boston, MA, Aug. 2003, pp. 385-388.
- [15] M.Guglielmi, P.Jarry, E.Kerhervé, O.Roquerbrun, and D.Schmitt "A new family of all-inductive dual-mode filters," *IEEE Transaction on Microwave Theory and Technique*, vol. 49, no. 10, pp. 1764-1769, Oct. 2001.
- [16] P.Savi, D.Trinchero, R.Tascone, and R.Orta "A new approach to the design of dual-mode rectangular waveguide filters with distributed coupling," *IEEE Transaction on Microwave Theory and Technique*, vol. 45, no. 2, pp. 221-228, Feb. 1997.
- [17] J.-F.Liang, X.-P.Liang, K.A.Zaki, and A.E.Atia "Dual-mode dielectric or air-filled rectangular waveguide filters," *IEEE Transaction on Microwave Theory and Technique*, vol. 42, no. 7, pp. 1330-1336, July. 1994.
- [18] A.E.Williams and A.E.Atia, "Dual-mode canonical waveguide filters," *IEEE Transaction on Microwave Theory and Technique*, vol. MTT-25, no. 12, pp. 1021-1026, Dec 1977.
- [19] C.Kdsia, R.Cameron, and W.-C.Tang, "Innovations in microwave filters and multiplexing networks for communications satellite systems," *IEEE Transaction on Microwave Theory and Technique*, vol. 40, no. 6, pp. 1133-1149, June 1992.
- [20] L.Accatino, G.Bertin, and M.Mongiardo, "Elliptical cavity resonators for dual-mode narrow-band filters," *IEEE Transaction on Microwave Theory and Technique*, vol. 45, no. 12, pp. 2393-2401, Dec. 1997.
- [21] A.E.Williams, "A Four-Cavity Elliptic Waveguide Filter," *IEEE Transaction on Microwave Theory and Technique*, vol. MTT-18, no. 12, pp. 1109-1114, Dec. 1970.
- [22] Y.C.Lee and C.S.Park, "A 60 GHz stripline BPF for LTCC system-in-package applications," in *2005 IEEE MTT-S Int. Microwave Sym. Dig.*, Long Beach, CA, June 2005, pp. 1413-1416.
- [23] Robert E. Collin, *Foundations for Microwave Engineering*, New York, NY/U.S.A: McGraw Hill, 1992.
- [24] I.Awai, A.C.Kundu, and T.Yamashita, "Equivalent-circuit representation and explanation of attenuation poles of a dual-mode dielectric-resonator bandpass filter," *IEEE Transaction on Microwave Theory and Technique*, vol. 46, no. 12, pp. 2159-2163, Dec. 1998.
- [25] J.-S. Hong and M.J.Lancaster, *Microstrip Filters for RF/Microwave Applications*, New York, NY/U.S.A: John Wiley & Sons, Inc., 2001.
- [26] M.Sagawa, K.Takahashi, and M.Makimoto, "Miniaturized hairpin resonator filters and their application to receiver front-end MIC's," *IEEE Transaction on Microwave Theory and Technique*, vol. 37, no. 12, pp. 1991-1997, May 1989.
- [27] J.B.Thomas, "Cross-coupling in coaxial cavity filters – a tutorial overview," *IEEE Transaction on Microwave Theory and Technique*, vol. 51, no. 4, pp. 1368-1376, April 2003.
- [28] L.K.Yeung and K.-L.Wu, "A compact second-order LTCC bandpass filter with two finite transmission zeros," *IEEE Transaction on Microwave Theory and Technique*, vol. 51, no. 2, pp. 337-341, Feb. 2003.
- [29] F.Purroy and L.Pradell, "New theoretical analysis of the LRRM calibration technique for vector network analyzers," *IEEE Transaction on Instrumentation and Measurement*, vol. 50, issues 5, pp. 1307-1314, Oct. 2001.
- [30] J.-H.Lee, N.Kidera, S.Pinel, J.Laskar, and M.M.Tentzeris, "A compact quasi-elliptic dual-mode cavity filter using LTCC technology for V-band WLAN gigabit wireless systems," presented at Proc. 36<sup>th</sup> European Microwave Conference, Manchester, U.K., 2006.
- [31] Jong-Hoon Lee, S. Pinel, J. Papapolymerou, J. Laskar, and M. M. Tentzeris, "Low-loss LTCC cavity filters using system-on-package technology at 60 GHz," *IEEE Trans. on Microwave Theory and Tech.*, vol. 53, no. 12, pp. 231-244, Dec. 2005.
- [32] K.A.Zaki, C.Chen, and A.E.Atia, "A circuit model of probes in dual-mode cavities," *IEEE Trans. Microwave Theory Tech.*, vol. 36, pp. 1740-1746, Dec. 1988.